https://doi.org/10.46813/2025-156-003

UDC 539:1, 42-43,669-1

EFFECT OF INERT GAS IONS IRRADIATION ON RADIATION DAMAGE OF HIGH-ENTROPY ALLOY $CrFe_2MnNi$ AND 18Cr10NiTi STEEL

I.V. Kolodiy, O.S. Kalchenko, M.A. Tikhonovsky, G.D. Tolstolutska
National Science Center "Kharkiv Institute of Physics and Technology", Kharkiv, Ukraine
E-mail: kolodiy@kipt.kharkov.ua

High-entropy alloys (HEAs) are of great interest as promising materials for use in nuclear reactors due to their exceptional mechanical properties, thermal stability, as well as corrosion and radiation resistance. In order to understand the effect of irradiation on the properties of HEAs and to demonstrate their potential advantages compared to conventional austenitic stainless steels, experiments on the irradiation of $CrFe_2MnNi$ HEA and 18Cr10NiTi steel (both with FCC lattice) with 20 keV He ions and 1.4 MeV Ar ions under identical conditions were conducted. Microstructure evolution of the irradiated materials and radiation-induced segregation of HEAs constituent elements were studied. It was found that the average size and density of cavities in 18Cr10NiTi steel are higher, and the swelling is almost twice as high compared to HEA.

INTRODUCTION

A necessary task for the development of new nuclear reactors with safe, stable and efficient properties is the study of structural materials under extreme conditions: high temperature, significant mechanical stress and intense irradiation. To predict the radiation resistance of new materials, their resistance to radiation swelling should be preliminarily assessed. And ion irradiation experiments using light and heavy ions are successfully used as an alternative to reactor irradiation.

Another serious problem both in fission and fusion reactors is the production of a certain amount of transmutation elements in structural materials through (n, p) and (n, α) reactions. High-energy α-particles may cause volume swelling by enhancing the nucleation and growth of cavities due to the low solubility of helium in metals [1].

Extensive studies of high-entropy alloys have revealed that they exhibit superior mechanical properties over a wide range of temperatures [2–8], as well as good corrosion resistance [9, 10]. In addition, HEAs are promising materials for nuclear energy – a number of studies (both theoretical and experimental) have shown that they are capable maintaining microstructural stability under intense ion irradiation [11–15]. However, the behavior of inert gases in HEAs, including the formation and growth of bubbles, is still insufficiently studied. In addition, up-to-date there is practically no works on the comparison of the radiation resistance of HEAs with commercial steels used in nuclear industry.

To understand the effects of irradiation on HEAs and demonstrate their potential advantages compared to industrial austenitic stainless steels, we conducted experiments on irradiation under identical conditions with Ar^+ and He^+ ions of $CrFe_2MnNi$ HEA and 18Cr10NiTi stainless steel with the same lattice type.

1. MATERIALS AND METHODS

Manufacturing of HEA ingots with the composition $CrFe_2MnNi$ (20Cr-40Fe-20Mn-20Ni composition in at.%) is described in details in [16]. Homogenization of ingots was carried out at 1050 °C for 24 h in pure argon atmosphere. After that, the alloy was thermo-mechanically treated by rolling at room temperature from 6 to 0.2 mm with intermediate annealing in argon at 1100 °C for 3 h. Final annealing after reducing the sample thickness to 0.2 mm also was performed at 1100 °C for 1 h in a purified argon atmosphere.

Commercial 18Cr10NiTi steel was annealed at 1050 °C for 30 min.

Samples for transmission electron microscopy (TEM) studies were prepared in the form of disks with a diameter of 3 mm. Thin foils were obtained by mechanical thinning of the disks to 130 μm with subsequent electropolishing and short-term annealing before irradiation.

Samples were irradiated with 1.4 MeV Ar^+ or 20 keV He^+ ions up to dose of $1 \cdot 10^{21}$ m^{-2}. Irradiation experiments were conducted in the accelerating-measuring system "ESU-2" [17]. The flux was $1 \cdot 10^{18}$ ions/($m^2 \cdot s$).

Temperature of samples during argon ions irradiation experiment was 600 °C.

Helium implantation was performed with a normal incident angle, and the temperature of samples did not exceed 25 °C. Microstructure evolution was studied during short-term post-irradiation annealing at 500 °C for 10 min.

The distributions of argon and helium ions and displacements per atom (dpa) were calculated using SRIM 2008 software [18]. Calculations of the irradiation dose (dpa) were based on the threshold displacement energy for each alloying element of 40 eV, as well as the Kinchin-Pease formalism and ASTM E521-96 recommendations [19, 20, 21] (Fig. 1).

The porous structure under argon ions irradiation should be dislocated in the near-surface region

(0…130 nm), since, as can be seen from the distribution profiles of ions range and defects, created by 1.4 MeV Ar^+ (see Fig. 1,a), exactly in this region inert gas practically does not accumulate and the structure evolution is caused only by displacement damage. According to the dose gradient through the thin foil, the average dose in this case is 30 dpa.

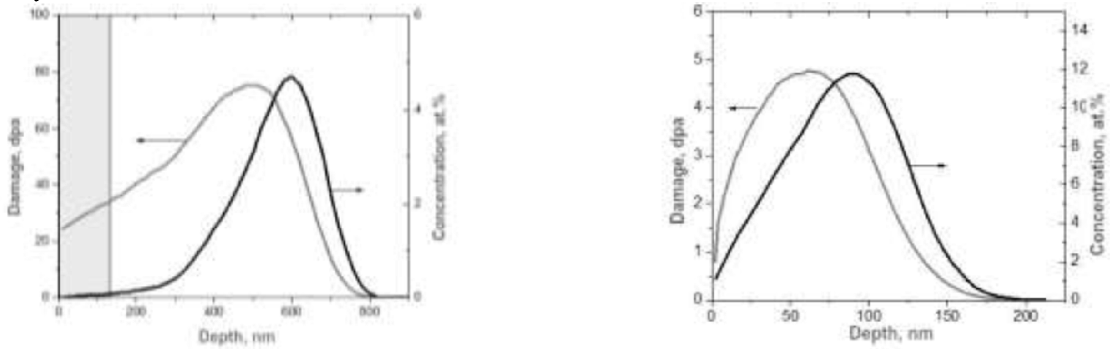

a *b*

Fig. 1. SRIM calculated injected ions distribution (black curve) and displacement damage (grey curve) of 1.4 MeV ions (a) and 20 keV He^+ ions (b) for irradiation dose of $1{\cdot}10^{21}$ ions/m^2. The area of TEM analysis is grayed (a)

TEM samples were thinned by electropolishing with a solution of 5% perchloric acid in ethanol from the back side of the sample to perforation. The thickness of TEM samples was determined using a convergent beam electron diffraction (CBED) pattern acquired in the two-beam approximation. The thickness estimation method, based on the comparison of the measured and simulated intensity profiles across the diffraction disc, is described in [22, 23].

The microstructure of steel and high-entropy alloy was studied by transmission electron microscopy. TEM method provides the ability to study microstructural changes in materials with a resolution of about 0.2 nm. Application of this method is determined, first of all, by the specifics of simulation experiments, where radiation damage is localized in a thin surface layer. All results were obtained using electron microscopes JEM-100CX and JEM-2100.

Typical initial microstructures of 18Cr10NiTi steel $CrFe_2MnNi$ HEA are shown in Fig. 2. Microstructure of 18Cr10NiTi steel (see Fig. 2,a) is presented mainly by coarse austenite grains with an average size of ~ 30 µm. Small δ-ferrite crystallites with volume fraction of 2…3% are also observed. Few annealing twins, second phase precipitations (titanium carbides and carbonitrides) and dislocations (with a density of ~ 10^8 cm^{-2}) were revealed in austenitic grains.

Initial microstructure of $CrFe_2MnNi$ HEA (see Fig. 2,b) is characterized by grain structure with an average grain size of > 10 µm. Practically, there were no any precipitations observed in high-entropy alloy.

XRD analysis showed that both alloys are single phase FCC alloys with lattice parameters of a = 3.592 Å in 18Cr10NiTi steel and a = 3.605 Å in $CrFe_2MnNi$ alloy, respectively.

Elemental composition of investigated alloys (nominal and measured by energy-dispersive X-ray spectrometry EDS) is shown in Table 1.

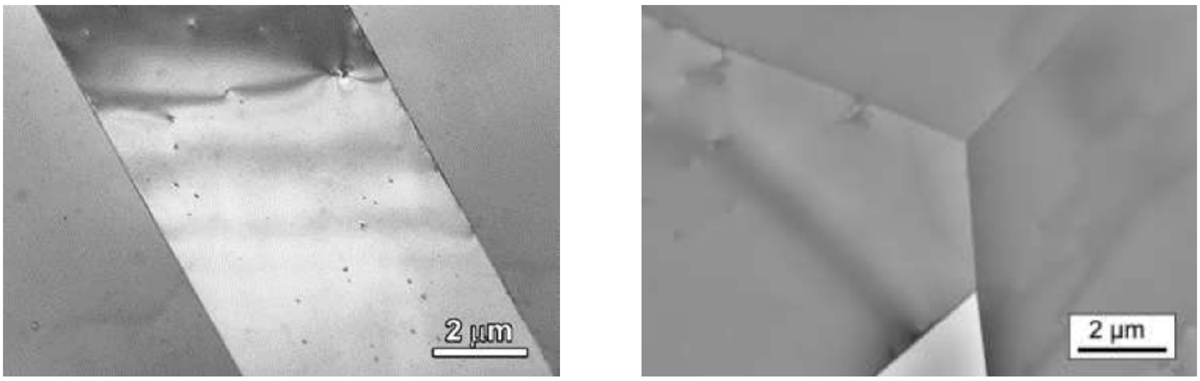

a *b*

Fig. 2. Initial microstructure of 18Cr10NiTi steel (a) and $CrFe_2MnNi$ HEA (b)

Table 1

Nominal and measured chemical compositions of studied alloys, wt.%

Compositions	Fe	Cr	Ni	Mn	Ti	Si
Cr-Fe-Mn-Ni						
Nominal	40	20	20	20	–	–
Measured	41.23	19.82	19.42	19.63	–	–
18Cr10NiTi						
Nominal	rest	17…19	9…11	2	0.4…1	0.8
Measured	68.1	17.9	10.8	1.75	0.71	0.74

Swelling investigation of studied materials was based on estimation of size and concentration of cavities, as well as character of their distribution. Total swelling was calculated using data on size and number of cavities.

Image processing and data analysis software was used to calculate swelling and plot histograms of cavities distribution by size.

Density of cavities was determined from EM images using the next equitation:

$$n = \frac{N}{V} = \frac{N}{A \cdot h}, \quad (1)$$

where n – density of cavities, m^{-3}; N – number of cavities; V – irradiated volume of material ($V = A \cdot h$), m^3; A – image area, m^2; h – foil thickness in the studied area of the sample, m.

Swelling S was calculated using formula [24]:

$$S = \frac{\Delta V}{V_0} \cdot 100\% = \frac{\Delta V}{V - \Delta V} \cdot 100\%, \quad (2)$$

where ΔV – change in material volume (numerically equal to total volume of cavities) after irradiation, m^3; V_0 – initial volume of material, m^3.

Total cavities volume ΔV was determined as the sum of volumes of all cavities, e.g.:

$$\Delta V = \frac{\pi}{6} \sum_{i=1}^{N} d_i^3, \quad (3)$$

where d_i – diameter of i-th cavity, m.

Dividing the numerator and denominator of expression (2) by V and substituting ΔV from (3) into (2), we finally obtain:

$$S = \frac{\frac{\pi}{6 \cdot A \cdot h} \sum_{i=1}^{N} d_i^3}{1 - \frac{\pi}{6 \cdot A \cdot h} \sum_{i=1}^{N} d_i^3} \cdot 100\%. \quad (4)$$

The sources of errors in calculating the swelling value are inaccuracies in determining the magnification (2%), sample thickness (10%), and cavities diameter (5%). As the result, the total error in determining the swelling was ~ 20%.

2. RESULTS AND DISCUSSIONS

2.1. NUCLEATION AND GROWTH OF POROSITY IN HIGH-ENTROPY ALLOY AND 18Cr10NiTi STEEL

The evolution of porosity in the high-entropy alloy $CrFe_2MnNi$ and austenitic stainless steel 18Cr10NiTi irradiated with energetic Ar^+ ions was investigated. In the near-surface region (0…130 nm) the damage dose was ~ 30 dpa with simultaneous implantation of argon to levels of 0.08 at.% at temperature of 600 °C. TEM studies showed that irradiation with 1.4 MeV Ar^+ ions is accompanied by the formation of defects such as cavities. Figs. 3, 4 show TEM images of Ar implanted samples of 18Cr10NiTi steel and HEA at a temperature of 600 °C.

The average size and density of cavities in 18Cr10NiTi steel are higher compared to those observed in $CrFe_2MnNi$ alloy. At the same time, the swelling in the HEA is almost two times less than in steel.

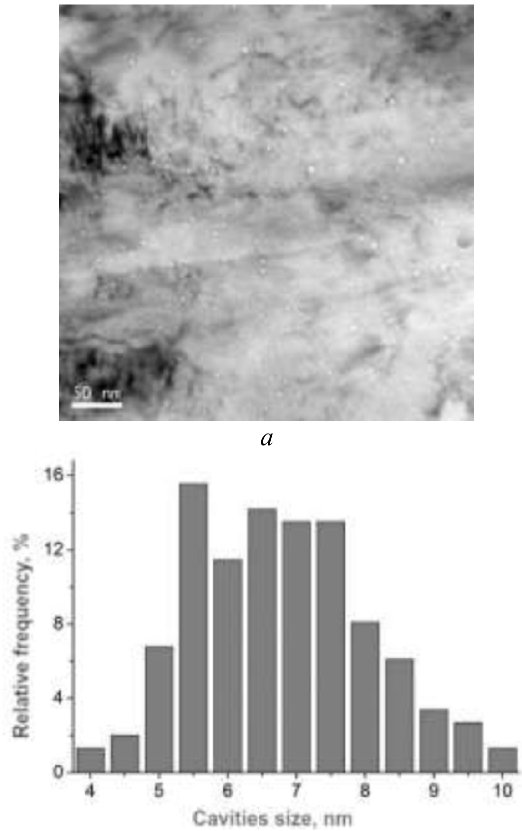

a

b

Fig. 3. TEM image of 18Cr10NiTi steel irradiated with Ar^+ ions to dose of 30 dpa at 600 °C (a) and distribution of cavities by size (b)

Estimated swelling of 18Cr10NiTi steel determined in this work has quite low value of 0.2%. Garner *et al.* [25] found that in steels, irradiated with neutrons in the EBR-II reactor, the swelling rate reaches up to ~ 1%/dpa in a wide temperatures range of 427…650 °C. However, this steady-state swelling stage is significantly delayed when the irradiation temperature is below 400 °C. The value of swelling strongly depends on the damage accumulation rate, as it was observed in 304 SS reflectors removed from EBR-II [26].

Now scientific community suggests that at temperatures of 290…340 °C the swelling rate limit may be ~ 0.07 %/dpa, and in some cases it is only ~ 0.003 %/dpa [27]. However, increasing the temperature above these values leads to a drastic increase in the swelling value by several times.

Regarding the HEAs swelling, it should be noted that their radiation swelling rate is much lower than that of conventional metals and alloys at the same value of radiation damage. This may be due to the three-dimensional diffusion behavior of interstitial clusters in HEAs, which increases the recombination rate of interstitial atoms and vacancies and inhibits the cavities nucleation [11, 28].

Higher resistance of HEAs to radiation swelling can also be explained by the local crystal lattice distortion, mixing entropy (low, medium and high entropy) and cocktail effects, as well as alloying with specific elements, which leads to the reduction in the size of cavities and their density [11, 29].

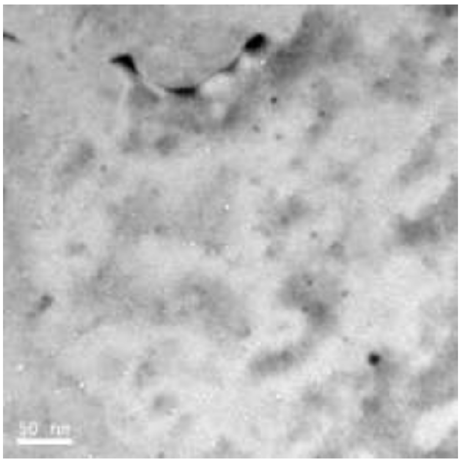

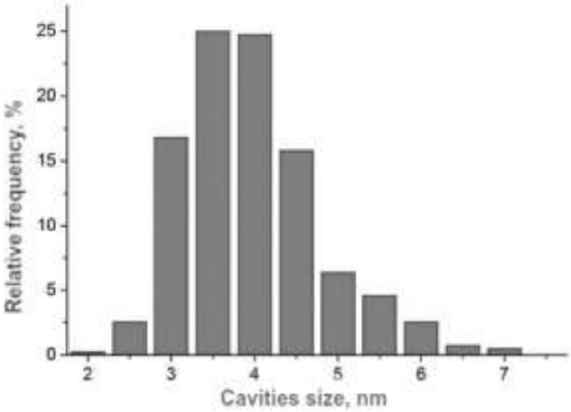

a *b*

Fig. 4. TEM image of $CrFe_2MnNi$ alloy irradiated with Ar^+ ions to dose of 30 dpa at 600 °C (a) and distribution of cavities by size (b)

2.2. EVOLUTION OF HELIUM BUBBLES IN $CrFe_2MnNi$ ALLOY AND 18Cr10NiTi STEEL DURING THE IRRADIATION AND ANNEALING PROCESSES

Quantitative characteristics of cavities or bubbles formation and subsequent swelling are often used as standards to compare the radiation resistance of different materials. The evolution of the microstructure was investigated after annealing of $CrFe_2MnNi$ alloy and 18Cr10NiTi steel irradiated at room temperature to a dose of 4.8 dpa and helium concentration of 11.7 at.%. Irradiation and annealing led to the formation of a high density of bubbles both in the HEA and steel.

Microstructures of 18Cr10NiTi steel and $CrFe_2MnNi$ HEA after annealing at 500 °C for 10 min in high vacuum are shown in Fig. 5.

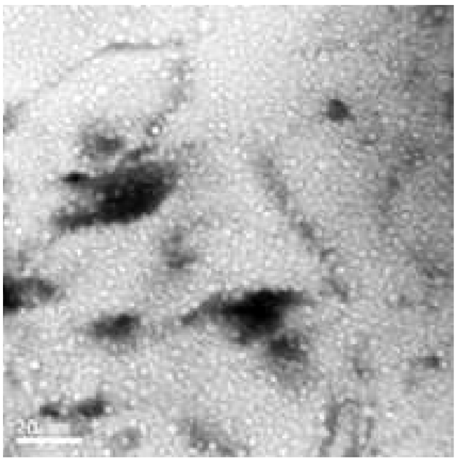

a

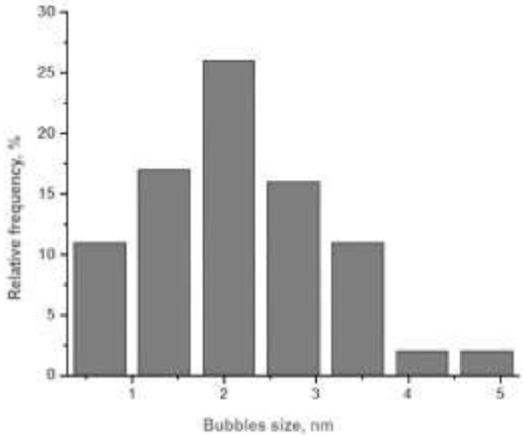

b

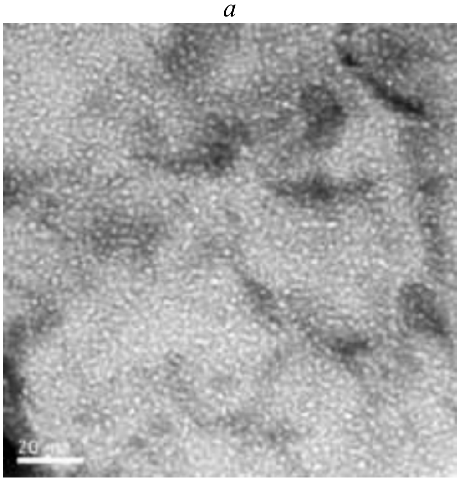

c

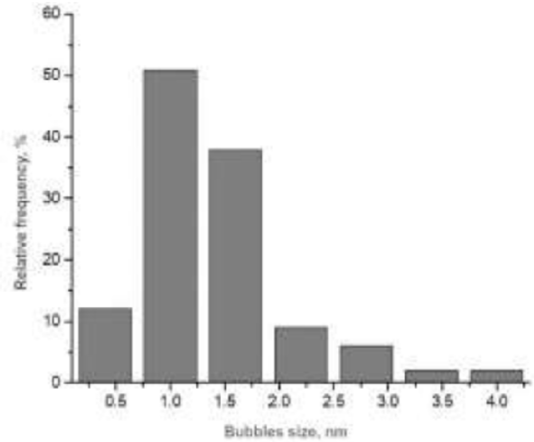

d

Fig. 5. Morphology and size distribution of He bubbles in irradiated ($1 \cdot 10^{21}$ m^{-2}) 18Cr10NiTi steel (a, b) and $CrFe_2MnNi$ alloy (c, d) after annealing at 500 °C for 10 min

Comparison of helium porosity parameters in these materials was carried out. The density and diameter of bubbles in both alloys, as well as their errors are summarized in Table 2. Comparison of these parameters shows that the size of helium bubbles in the $CrFe_2MnNi$ alloy is smaller than in 18Cr10NiTi steel – (1.1 ± 0.3) nm and (2.1 ± 0.4) nm, respectively, but their density is approximately 3 times higher.

Table 2

Average size and density of He bubbles in 18Cr10NiTi steel and $CrFe_2MnNi$ alloy after irradiation and annealing at 500 °C

Material	Average diameter, nm	Density, 10^{24} m^{-3}	Swelling, %
$CrFe_2MnNi$	1.1 ± 0.3	3,5 ± 0.5	0.22
18Cr10NiTi	2.1 ± 0.4	1.1 ± 0.2	0.48

Calculated values of He induced swelling are 0.22 and 0.48% in HEA and steel, respectively. Obtained result indicates that $CrFe_2MnNi$ alloy is much more resistant to the formation of helium bubbles than 18Cr10NiTi stainless steel.

Mechanisms of He porosity suppression in HEAs was discussed by Zhanfeng et al. [30]. Based on this consideration the following can be stated. Under irradiation a significant lattice distortion occurs both in the HEA and the steel. However, the potential energy gap between two neighboring positions in the $CrFe_2MnNi$ lattice is quite large compared to ideal zero, for example, in pure nickel. Helium in $CrFe_2MnNi$ alloy is affected by strong fluctuations in the lattice potential energy during frequent jumps in the process of diffusion and cluster formation. As a result, most of the helium atoms can be trapped and will not participate in the bubble nucleation process. This confirms the mechanism of radiation resistance of HEAs with respect to the development of helium porosity and indicates that slow diffusion process and severe lattice distortion provide deeper sites for He atoms trapping. Due to the complicated migration of the He atoms, the process of helium bubble nucleation in HEA is slowed down.

Study of the inert gas bubbles nucleation and growth in Ni-based concentrated solid solutions, containing different types and amounts of elements, showed that although increasing the chemical complexity of the alloy assists in suppressing the bubbles nucleation in general, but there is no monotonic relationship between the bubble growth rate and the number of alloying elements. Certain elements (e.g., Fe and Pd) are more effective in suppressing bubble growth than others (e.g., Cr and Mn) [31]. In particular, high mobility of vacancies through Cr sites leads to a large flow of vacancies and an increase in bubble size, while significant degree of atomic size mismatch caused by Pd assists in deflecting the flow of vacancies away from the bubbles and therefore reduces swelling. The effects revealed in [31] provide new strategies for designing high-entropy alloys with enhanced swelling resistance.

2.3. RADIATION-INDUCED SEGREGATION OF ELEMENTS IN $CrFe_2MnNi$ ALLOY

The process of micro-chemical evolution of a homogeneous solid solution, which is determined by the interaction of fluxes of point defects and dissolved atoms, drastically changes the chemical composition homogeneity of the irradiated steels. It is very important that change in matrix composition as a result of radiation-induced segregation (RIS) leads to a change in the main parameters which determine the behavior of radiation swelling:

– energy and geometric characteristics of point defects and their complexes;

– concentration and strength of point defects sinks.

The porosity evolution in each local region of the irradiated material can proceed in its own way. In HEAs different elements are randomly distributed in a simple crystal structure, such as face-centered cubic (fcc), creating a unique distortion for each lattice region and a chemically complex environment around each atom [11, 12]. Studies have shown that chemical complexity can be used for effective tuning of the defect energy landscape, promoting defect recombination, and improving the radiation resistance of materials [32, 33].

Figs. 6, 7 shows STEM images of the structure and EDS mapping of the $CrFe_2MnNi$ high-entropy alloy in the initial state and after irradiation with 1.4 MeV Ar^+ ions at 600 °C. In both cases, only a uniform distribution of elements is observed, i.e., after irradiation with argon ions, radiation-induced segregation in the alloy was not detected.

In the case of irradiation of the $CrFe_2MnNi$ alloy with helium ions and subsequent annealing at 500 °C, although segregation processes were observed, but in an implicit form. As can be seen from Fig. 8, isolated cavities (bubbles) and precipitates, as well as bubble-precipitate complexes, are observed in the irradiated samples, demonstrating the absence of any regularity in the bubbles distribution. This indicates that bubbles and second-phase precipitates nucleate independently; and only during the growth process, under the influence of irradiation and subsequent annealing, the formation of such complexes occurs. EDS maps reveal a slight segregation of only chromium atoms.

The appearance of chromium-enriched regions may indicate the formation of σ-phase in the alloy. It is known that in homogeneous CrMnFeCoNi HEA with a similar composition and structure, a chromium-rich σ-phase can form during prolonged annealing in the temperature range of 600…800 °C [34]. At the same time, introducing defects into the alloy by deformation significantly accelerates this process, and the sigma-phase is observed after annealing at 600 °C for 1 h [35]. It can be assumed that defects, formed under the irradiation with He^+ ions, also significantly accelerate diffusion processes and lead to the decomposition of the solid solution in the $CrFe_2MnNi$ alloy, which is most likely non-equilibrium at this temperature.

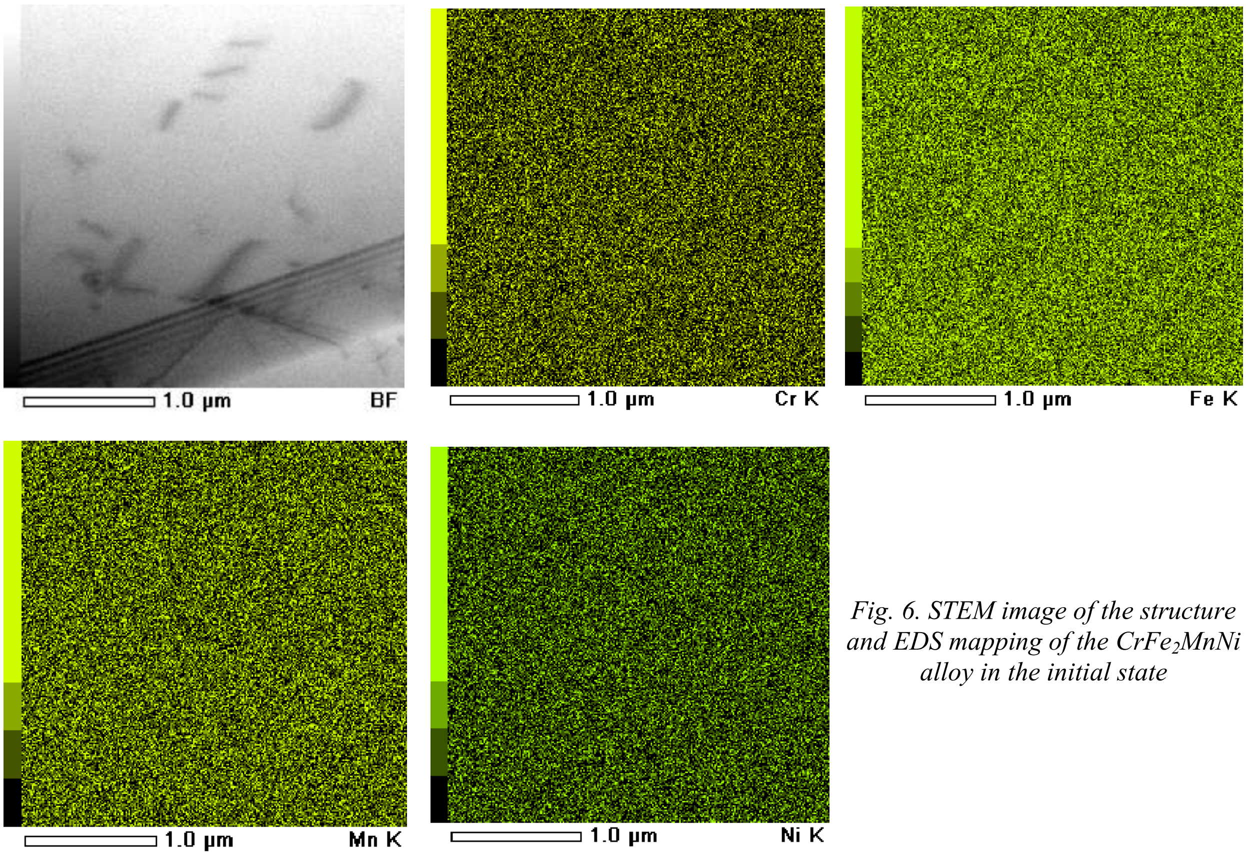

Fig. 6. STEM image of the structure and EDS mapping of the $CrFe_2MnNi$ alloy in the initial state

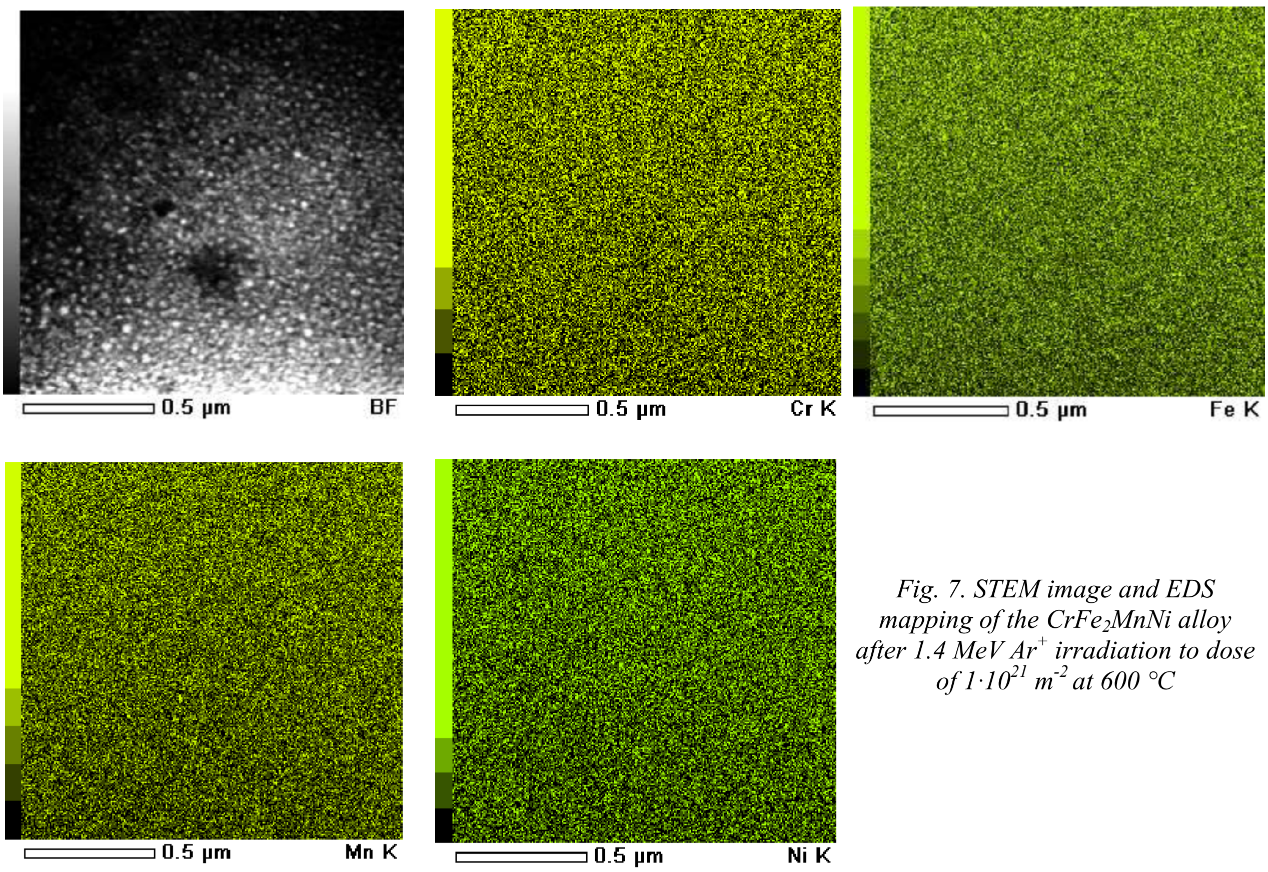

Fig. 7. STEM image and EDS mapping of the $CrFe_2MnNi$ alloy after 1.4 MeV Ar^+ irradiation to dose of $1\cdot10^{21}$ m^{-2} at 600 °C

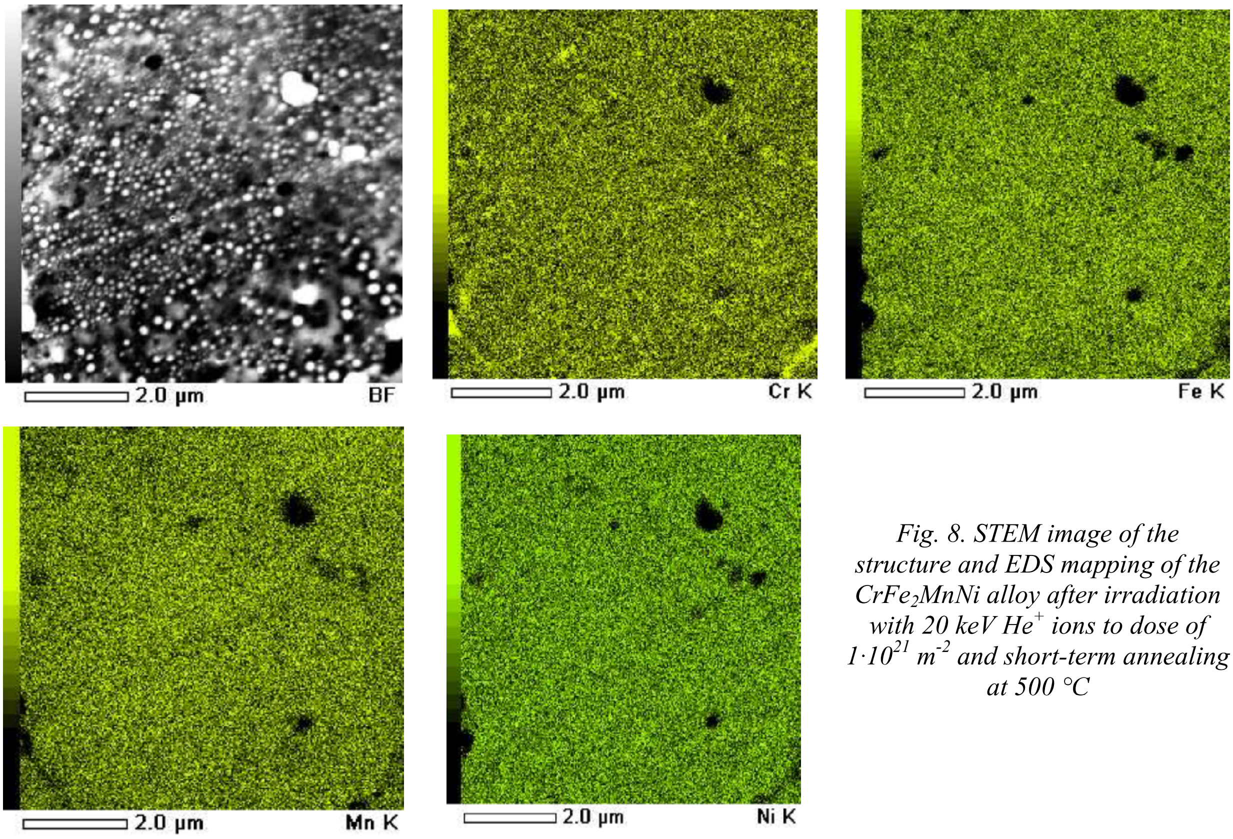

Fig. 8. STEM image of the structure and EDS mapping of the $CrFe_2MnNi$ alloy after irradiation with 20 keV He^+ ions to dose of $1{\cdot}10^{21}$ m^{-2} and short-term annealing at 500 °C

But there is also a more "subtle" mechanism for the appearance of chromium-rich regions. Due to the extremely low solubility in most solids, helium atoms quickly cluster with vacancies, forming helium-stabilized cavities or bubbles, which deteriorate the thermo-mechanical properties of materials. It is known that radiation-induced segregation of point defects at the sinks is determined by the parameters of diffusion of matrix atoms via vacancies from the sink and the parameters of diffusion of interstitial atoms toward the sink. These two mechanisms can compete with each other or work together. The outflow of material atoms (for example, Fe, Cr, Ni, Mn) is carried out via vacancies, moving to the growing cavity, while at the same time, diffusion of the same elements via the interstitials occurs towards this flux. The ratio of these fluxes by different mechanisms exactly determines the segregation of the elements in the solid solution [12, 33, 36].

Wang et al. [31] investigated the effect of the numbers and type of alloying elements on the bubble nucleation process in the concentrated solid solution alloys. The main driving force for bubble growth is the flux of vacancies to the bubble surface. Since vacancies usually prefer to diffuse via certain alloying elements, the flux of vacancies is often non-stoichiometric, leading to either enrichment or depletion of certain elements around the bubbles [37–39]. High mobility of vacancies through Cr sites leads to a large flux of vacancies and an increase in bubble size. At the same time, the rapid diffusion of chromium (the smallest atom in alloy) leads to the segregation of this element at the cavity/bubble surface [40].

For a clearer understanding of the role of alloy non-equilibrium in the formation of chromium-rich regions, experiments should be performed on more equilibrium alloys with reduced chromium concentration.

In general, the segregation tendencies observed in HEAs are qualitatively similar but less pronounced in magnitude compared to the behavior of austenitic stainless steels [41]. It is important to note that, unlike conventional alloys, HEAs have no principal element that dominates in the solid solution composition. Therefore, the influence of other effects, such as competing RIS kinetics of solid solutions, high entropy and severe lattice distortion, which are less pronounced in many conventional alloys, may increase the complexity of RIS processes in HEAs. So, the suppression of radiation-induced segregation observed in this study may be due to the reasons mentioned above.

CONCLUSIONS

1. The evolution of porosity in the $CrFe_2MnNi$ high-entropy alloy and 18Cr10NiTi steel was investigated in the dose range up to 30 dpa with simultaneous argon implantation to 0.08 at.% at temperature of 600 °C. It was found that the average size and density of cavities in 18Cr10NiTi steel are higher, and swelling is almost twice as high compared to $CrFe_2MnNi$ HEA.

2. $CrFe_2MnNi$ alloy was found to be much more resistant to He bubbles formation than 18Cr10NiTi stainless steel, suggesting that retarding of the diffusion process and significant lattice distortion provide deeper sites for He atoms trapping.

3. The suppression of radiation-induced segregation observed in this study can be caused by the competing kinetics of RIS in solid solutions, high mixing entropy and severe lattice distortion.

REFERENCES

1. H. Ullmaier. The influence of helium on the bulk properties of fusion reactor structural materials // *Nucl. Fusion*. 1984, v. 24, N 8, p. 1039-1065; DOI: 10.1088/0029-5515/24/8/009

2. D.B. Miracle, O.N. Senkov. A critical review of high entropy alloys and related concepts // *Acta Materialia*. 2017, v. 122, p. 448-511; DOI: 10.1016/j.actamat.2016.08.081

3. Z. Li, K. Pradeep, Y. Deng, D. Raabe, C.C. Tasan. Metastable high-entropy dual-phase alloys overcome the strength-ductility trade-off // *Nature.* 2016, v. 534, p. 227-230; DOI: 10.1038/nature17981

4. F. Otto, A. Dlouhy, C. Somsen, H. Bei, G. Eggeler, E.P. George. The influences of temperature and microstructure on the tensile properties of a CoCrFeMnNi high-entropy alloy // *Acta Mater*. 2013, v. 61, p. 5743-5755;
DOI:10.1016/j.actamat.2013.06.018

5. Z. Li, S. Zhao, R. Ritchie, M. Meyers. Mechanical properties of high-entropy alloys with emphasis on face-centered cubic alloys // *Progress in Materials Science*. 2019, v. 102, p. 296-345;
DOI: 10.1016/j.pmatsci.2018.12.003

6. A. Manzonia, U. Glatzel. New multiphase compositionally complex alloys driven by the high entropy alloy approach // *Materials Characterization.* 2019, v. 147, p. 512-532;
DOI: 10.1016/j.matchar.2018.06.036

7. B. Gludovatz, A. Hohenwarter, D. Catoor, E.H. Chang, E.P. George, R.O. Ritchie. A fracture-resistant high-entropy alloy for cryogenic applications // *Science*. 2014, v. 345, p. 1153-1158;
DOI: 10.1126/science.1254581

8. B. Gludovatz, A. Hohenwarter, K. Thurston, et al. Exceptional damage-tolerance of a medium-entropy alloy CrCoNi at cryogenic temperatures // *Nature Communications.* 2016, v. **7**, p. 10602;
DOI: 10.1038/ncomms10602

9. Y. Qiu, S. Thomas, M.A. Gibson, et al. Corrosion of high entropy alloys // *NPJ Mater. Degrad*. 2017, v. 1, p. 15; DOI: 10.1038/s41529-017-0009-y

10. A.V. Levenets, M.A. Tikhonovsky, V.N. Voyevodin, et al. High-entropy alloys as a prospective class of new radiation-tolerant materials. Research development analysis based on the information databases // *PAST.* 2021, N 2 (132), p. 3-15; DOI: 10.46813/2021-132-003

11. Y. Zhang, T. Egami, W.J. Weber. Dissipation of radiation energy in concentrated solid-solution alloys: Unique defect properties and microstructural evolution // *MRS Bulletin*. 2019, v. 44 (10), p. 798-811;
DOI: 10.1557/mrs.2019.233

12. Y. Zhang, S. Zhao, W.J. Weber, et al. Atomic-level heterogeneity and defect dynamics in concentrated solid-solution alloys // *Curr. Opin. Solid State Mater. Sci*. 2017, v. 21 (5), p. 221-237;
DOI: 10.1016/j.cossms.2017.02.002

13. S. Zhao, D. Chen, J. Kai. First-principles study of He behavior in a NiCoFeCr concentrated solid-solution alloy // *Materials Research Letters*. 2019, v. 7(5), p. 188-193;
DOI: 10.1080/21663831.2019.1574926

14. W. Chen, X. Liu, Y. Chen, J. Yeh, K. Tseng, K. Natesan. Irradiation effects in high entropy alloys and 316H stainless steel at 300 °C // *Journal of Nuclear Materials*. 2018, v. 510, p. 421-430;
DOI: 10.1016/j.jnucmat.2018.08.031

15. S. Liu, W. Lin, D. Chen, B. Han, S. Zhao, F. He, H. Niu, J. Kai. Effects of temperature on helium cavity evolution in single-phase concentrated solid-solution alloys // *Journal of Nuclear Materials*. 2021, v. 557, p. 153261; DOI: 10.1016/j.jnucmat.2021.153261

16. I.V. Kolodiy, O.M. Velikodnyi, M.A. Tikhonovsky, V.N. Voyevodin, O.S. Kalchenko, R.L. Vasilenko, V.S. Okovit. Microstructure and mechanical properties of oxide dispersion strengthened high-entropy alloys CoCrFeMnNi and $CrFe_2MnNi$ // *PAST.* 2021, N 2(132), p. 87-94; DOI: 10.46813/2021-132-087

17. G.D. Tolstolutskaya, V.V. Ruzhytskiy, I.E. Kopanetz, V.N. Voyevodin, A.V. Nikitin, S.A. Karpov, A.A. Makienko, T.M. Slusarenko. Accelerating complex for study of helium and hydrogen behavior in conditions of radiation defects generation // *PAST*. 2010, N 4(65), p. 135-140.

18. SRIM (2008), http://www.srim.org.

19. R. Stoller, M. Toloczko, G. Was, A. Certain, S. Dwaraknath, F. Garner. On the use of SRIM for computing radiation damage exposure // *Nucl. Instrum. Methods Phys. Res. Sect. B Beam Interact. Mater. Atoms*. 2013, v. 310, p. 75-80;
DOI: 10.1016/j.nimb.2013.05.008

20. ASTM E521-96, 2009, ASTM. DOI: 10.1520/E0521-96R09E01

21. M. Bratchenko, V. Bryk, S. Dyuldya, A. Kalchenko, N. Lazarev, V. Voyevodin. Comments on DPA calculation methods for ion beam driven simulation irradiations // *PAST*. 2013, N 2 (84), p.11-16.

22. M. Klinger. More features, more tools, more CrysTBox // *J. Appl. Cryst*. 2017, v. 50, p. 1226-1234;
DOI: 10.1107/S1600576717006793

23. S. Karpov, G. Tolstolutskaya, A. Kalchenko. Effect of noble-gas bubbles on deuterium trapping behavior in argon pre-implanted stainless steel // *Journal of Nuclear Materials*. 2022, v. 566, p. 153661;
DOI: 10.1016/j.jnucmat.2022.153661

24. V.V. Bryk, V.N. Voyevodin, A.S. Kalchenko, V.V. Melnichenko, I.M. Neklyudov, V.S. Ageev, A.A. Nikitina. Swelling of dispersion strengthened by yttrium oxides steel 018Cr10NiTi irradiated by heavy ions // *PAST*. 2013, N 2(84), p. 23-30.

25. F. Garner, M. Toloczko, B. Sencer. Comparison of swelling and irradiation creep behavior of fcc-austenitic and bcc-ferritic/martensitic alloys at high neutron exposure // *J. Nucl. Mater*. 2000, v. 276, p. 123-142; DOI: 10.1016/S0022-3115(99)00225-1

26. F. Garner, B. Makenas. Recent experimental results on neutron-induced void swelling of AISI 304 stainless steel concerning its interactive dependence on temperature and displacement rate // *Fontevraud-6 Symposium on Contribution of Materials Investigations to Improve the Safety and Performance of LWRs*. 2006, p. 18-22.

27. M. Song, K.G. Field, R.M. Cox, G.S. Was. Microstructural characterization of cold-worked 316

stainless steel flux thimble tubes irradiated up to 100 dpa in a commercial Pressurized Water Reactor // *J. Nucl. Mater.* 2020, v. 541, p. 152400;
DOI: 10.1016/j.jnucmat.2020.152400

28. C. Lu, L. Niu, N. Chen, et al. Enhancing radiation tolerance by controlling defect mobility and migration pathways in multicomponent single-phase alloys // *Nature Communications*. 2016, v. **7**, p. 13564;
DOI: 10.1038/ncomms13564

29. K. Jin, C. Lu, L.M. Wang, J. Qu, W.J. Weber, Y. Zhang, H. Bei. Effects of compositional complexity on the ion-irradiation induced swelling and hardening in Ni-containing equiatomic alloys // *Scripta Materialia*. 2016, v. 119, p. 65-70;
DOI: 10.1016/j.scriptamat.2016.03.030

30. Y. Zhanfeng, L. Shaoshuai, X. Songqin, Y. Zhang, Y. Wang, T. Yang. He behavior in Ni and Ni-based equiatomic solid solution alloy // *J. Nucl. Mater.* 2018, v. 505, p. 200-206;
DOI: 10.1016/j.jnucmat.2018.04.009.

31. X. Wang, K. Jin, C.Y. Wong, et al. Understanding effects of chemical complexity on helium bubble formation in Ni-based concentrated solid solution alloys based on elemental segregation measurements // *J. Nucl. Mater.* 2022, v. 569, p. 153902;
DOI: 10.1016/j.jnucmat.2022.153902

32. O. El-Atwani, N. Li, M. Li, et al. Outstanding radiation resistance of tungsten-based high-entropy alloys // *Sci. Adv*. 2019, v. 5 (3), p. 1-9;
DOI: 10.1126/sciadv.aav2002

33. T. Yang, C. Li, S.J. Zinkle, S. Zhao, H. Bei, Y. Zhang. Irradiation responses and defect behavior of single-phase concentrated solid solution alloys // *J. Mater. Res*. 2018, v. 33, p. 3077-3091;
DOI: 10.1557/jmr.2018.285

34. E.J. Pickering, R. Muñoz-Moreno, H.J. Stone, N.G. Jones. Precipitation in the equiatomic high-entropy alloy CrMnFeCoNi // *Scr. Mater*. 2016, #113, p. 106-109; DOI: 10.1016/j.scriptamat.2015.10.025

35. N.D. Stepanov, D.G. Shaysultanov, M.S. Ozerov, et al. Second phase formation in the CoCrFeNiMn high entropy alloy after recrystallization annealing // *Materials Letters*. 2016, N 185, p. 1-4;
DOI: 10.1016/j.matlet.2016.08.088

36. G.S. Was. *Fundamentals of Radiation Materials Science: Metals and Alloys*. Springer, 2017. ISBN: 978-1-4939-3436-2 (Print) 978-1-4939-3438-6; DOI: 10.1007/978-1-4939-3438-6

37. A.J. Ardell, P. Bellon. Radiation-induced solute segregation in metallic alloys // *Curr. Opin. Solid State Mater. Sci.* 2016, v. 20, p. 115-139;
DOI: 10.1016/j.cossms.2015.11.001

38. K.G. Field, L.M. Barnard, C.M. Parish, J.T. Busby, D. Morgan, T.R. Allen. Dependence on grain boundary structure of radiation induced segregation in a 9 wt.% Cr model ferritic/martensitic steel // *J. Nucl. Mater*. 2013, v. 435, p. 172-180;
DOI: 10.1016/j.jnucmat.2012.12.026

39. P.R. Okamoto, L.E. Rehn. Radiation-induced segregation in binary and ternary alloys // *J. Nucl. Mater*. 1979, v. 83, p. 2-23;
DOI: 10.1016/0022-3115(79)90587-7

40. Y.N. Osetsky, L.K. B´eland, A.V. Barashev, Y. Zhang. On the existence and origin of sluggish diffusion in chemically disordered concentrated alloys // *Curr. Opin. Solid State Mater.* 2018, v. 22(3), p. 65-74;
DOI: 10.1016/j.cossms.2018.05.003

41. N.A.P. Kiran Kumar, C. Li, K.J. Leonard, H. Bei, S.J. Zinkle. Microstructural stability and mechanical behavior of FeNiMnCr high entropy alloy under ion irradiation // *Acta Materialia*. 2016, v. 113, p. 230-244; DOI: 10.1016/j.actamat.2016.05.007

Article received 10.03.2025

ВПЛИВ ОПРОМІНЕННЯ ПРИСКОРЕНИМИ ІОНАМИ ІНЕРТНИХ ГАЗІВ НА РАДІАЦІЙНЕ ПОШКОДЖЕННЯ ВИСОКОЕНТРОПІЙНИХ СПЛАВІВ $CrFe_2MnNi$ ТА СТАЛІ Х18Н10Т

І.В. Колодій, О.С. Кальченко, М.А. Тихоновський, Г.Д. Толстолуцька

Високоентропійні сплави (ВЕС) розглядаються як перспективні матеріали для застосування в ядерних реакторах через їх багатообіцяючі механічні властивості, корозійну та радіаційну стійкості. З метою розуміння впливу опромінення на властивості ВЕС і демонстрації їх потенційних переваг, як порівнювати зі звичайними аустенітними нержавіючими сталями, проведено експерименти з опромінення в ідентичних умовах ВЕС $CrFe_2MnNi$ та сталі Х18Н10Т іонами гелію з енергією 20 кеВ та іонами аргону з енергією 1,4 МеВ. Досліджено еволюцію мікроструктури опромінених матеріалів та радіаційно-індуковану сегрегацію складових елементів ВЕС. Встановлено, що середній розмір та щільність порожнин у сталі Х18Н10Т вищі, а розпухання майже у два рази більше порівняно із ВЕС.